Chinese Chemical Letters 34 (2023) 108085

Contents lists available at ScienceDirect

Chinese Chemical Letters

journal homepage: www.elsevier.com/locate/cclet

Optimizing the electronic structure of Fe-doped Co_3O_4 supported Ru catalyst *via* metal-support interaction boosting oxygen evolution reaction and hydrogen evolution reaction

Li Gao[a,b,c,1], Xia Zhong[a,b,1], Junnan Chen[a,b], Ying Zhang[a,d], Jie Liu[a,e], Bingsen Zhang[a,b,*]

[a] Shenyang National Laboratory for Materials Science, Institute of Metal Research, Chinese Academy of Sciences, Shenyang 110016, China
[b] School of Materials Science and Engineering, University of Science and Technology of China, Shenyang 110016, China
[c] Nano Science and Technology Institute, University of Science and Technology of China, Suzhou 215123, China
[d] School of Petrochemical Engineering, Liaoning Petrochemical University, Fushun 113001, China
[e] Department of Chemistry, College of Science, Northeastern University, Shenyang 110819, China

ARTICLE INFO

Article history:
Received 19 November 2022
Revised 8 December 2022
Accepted 16 December 2022
Available online 19 December 2022

Keywords:
Metal-support interaction
Fe doping
Electronic structure
OER
HER

ABSTRACT

Metal-support interaction (MSI) is an efficient way in heterogeneous catalysis and electrocatalysis to modulate the electronic structure of metal for enhanced catalytic activity. However, there are still great challenges in promoting the hydrogen evolution reaction (HER) and oxygen evolution reaction (OER) simultaneously by this way. Herein, Fe-doped Co_3O_4 supported Ru (Ru/FeCo) catalysts are synthesized by MSI strategies to further improve the electrocatalytic activity and stability of the catalysts. The results show that the optimized Ru/FeCo catalyst exhibits the best catalytic performance. The HER and OER tests at 10 mA/cm^2 in 1 mol/L KOH solution show excellent overpotentials of 155 mV and 283 mV, respectively. The activity and stability enhancement can be attributed to the MSI that effectively modify the electronic structure and improve interfacial electron transfer between Ru and Fe-doped Co_3O_4 (FeCo). This work provides an innovative direction for the design of high-efficiency bifunctional electrocatalysts by virtue of the MSI.

Electrolysis of water is one of the most promising methods for storing and utilizing renewable energy sources in the form of clean chemicals [1,2]. However, hydrogen evolution reaction (HER) and oxygen evolution reaction (OER) as two half-reactions for the electrochemical water splitting may be kinetically sluggish due to involved multiple proton-coupled electron transfer [3]. Utilizing the interaction between the metal and the support, so-called metal-support interaction (MSI), is one of the most essential strategies to enhance electrocatalytic efficiency due to structural and synergetic promotion [4]. To be specific, MSI contains the electronic, geometric and bifunctional effects [5], among which electronic effects play the most important role in exploring bifunctional electrocatalysts to accelerate the process of HER and OER effectively. However, the performance of bifunctional electrocatalysts and the utilization efficiency of noble metals still have much room for improvement so far. Therefore, it is urgent to take advantage of MSI to further enhance the catalytic properties.

Currently, non-platinum noble metals including Ru, Rh and Ir have always been attracted in electrochemical hydrogen production research [6]. Among them, Ru has attracted much attention because of its low cost (1/3 of the price of Pt), high catalytic activity and excellent stability [7]. But, due to the large cohesive energy, Ru nanoparticles (NPs) are prone to aggregate, resulting in reduced activity [8]. So, uniformly dispersing or loading Ru NPs on low-cost support materials with high electrical conductivity is considered as a promising strategy to further reduce the cost of Ru-based electrocatalyst while maintaining its high HER activity [9]. In previous studies, Sun *et al.* [10] proved that high dispersion of the ultrasmall Ru NPs in Ru/S-rGO could increase the active surface area of the electrocatalyst, enhance the MSI, and thus improve the catalysis activity for HER under alkaline conditions. Liu *et al.* [11] loaded Ru nanoclusters on porous Co_3O_4 nanowires (NWs), and the obtained Ru/Co_3O_4 NWs have better HER performance in alkaline medium.

Transition metal oxide Co_3O_4 is a spinel oxide, which is considered as a promising non-noble metal electrocatalyst with the advantages of low cost, abundant reserves, and good durability [12–

* Corresponding author at: Shenyang National Laboratory for Materials Science, Institute of Metal Research, Chinese Academy of Sciences, Shenyang 110016, China.
E-mail address: bszhang@imr.ac.cn (B. Zhang).
[1] These authors contributed equally to this work.

https://doi.org/10.1016/j.cclet.2022.108085
1001-8417/

15]. It is often used for OER in alkaline media. However, due to its poor intrinsic activity, the catalytic performance is lower than most advanced OER catalysts. Therefore, it is promising to modify Co_3O_4 to improve its catalytic performance in OER. Making the efforts to modify the electronic structure of catalysts is one of the most efficient strategies to systematically improve the intrinsic OER activity [16–19], this is due to 3d orbital electronic configuration plays a decisive role in the influence of binding energy of OER intermediates on the oxide surface. Yan *et al.* [20] engineered the electronic structure of Co_3O_4 by carbon-doping. As a result, the as-prepared C–Co_3O_4 exhibited low overpotential along with good stability in alkaline media for both HER and OER. Yan *et al.* [21] doped Ag ion into Co_3O_4 nanosheets to improve the ratio of the active sites (Co^{2+}) and obtained high efficiency OER electrocatalyst in acidic electrolyte. Furthermore, as the redox characteristics of Fe is switchable between +3 and +2 oxidation states, Fe-doping may contribute better electrochemical performance to the Co_3O_4 [22]. Many studies have reported that Fe^{3+} incorporation in cobalt oxide could trigger a spin state change at the neighboring Co^{3+} and elongation of the Co^{3+}-O bond and resulting better activity in OER. Budiyanto *et al.* [23] proved that incorporating a small amount of iron in cobalt oxide was beneficial to enhance the OER activity by inducing lower charge transfer resistance, an increase of the $Co^{2+}{}_{(Td)}$ sites, and formation of open mesopores structures. Gao *et al.* [24] introduced high spin state Fe^{3+} into octahedral sites controllably to regulate the valence state of Co^{3+} to optimized OER activity.

In the view of above considerations, Fe-doped Co_3O_4 in an ordered mesoporous morphology as an efficient solid support for hosting ultra-small Ru NPs (~1.48 nm) for the HER and OER was shaped. Our research revealed that the Ru/FeCo, as a bifunctional electrocatalyst, not only shows excellent overpotentials of 155 mV (10 mA/cm^2) for HER and 283 mV (10 mA/cm^2) for OER, respectively, but also has excellent long-term electrochemical durability. More importantly, we found that incorporating Fe in Co_3O_4 resulted in a decrease in the NWs' array length and increase in the number of active sites Co^{2+} and defective oxygen species. Furthermore, comparing to the Ru/Co_3O_4, the MSI in Ru/FeCo improves electron transfer between Ru NPs and supports, which helps Ru atoms keep in electron-rich state and is beneficial to enhance its catalytic activity. All in all, this work provides an innovative direction for the design of high-efficiency bifunctional electrocatalysts by virtue of the interactions between active metals and metal-oxide supports.

Co_3O_4, FeCo, Ru/Co_3O_4 and Ru/FeCo with pure phase and good crystallinity were examined by XRD. The typical diffraction peaks (Fig. S1a in Supporting information) of Co_3O_4 at $2\theta = 31.27^\circ$, 36.85°, 44.81°, 59.35° and 65.23° can be indexed to (220), (311), (400), (511) and (440) planes (JCPDS No. 74-2120). There were no Fe-related peaks were detected excepted high lattice expansion in spinel structures, as evidenced by the 0.20° shift to left of the (440) peaks in Fig. S1b (Supporting information). Furthermore, the crystalline phase of Co_3O_4 and FeCo did not change after the introduction of Ru through cation exchange and the subsequent reduction at 125 °C in 10% H_2/Ar atmosphere.

TEM characterization was performed to visualize the morphology and topography of the samples (Figs. 1a–d) [25,26]. It can be seen that Co_3O_4 showed mesostructured NW morphology with a high degree of order. With the incorporation of Fe, the length of the NWs decreased while the disorder increased. As shown in Figs. 1c and d, ultra-small Ru NPs with the size of *ca.* 1.48 nm are uniformly dispersed on the pure Co_3O_4 and Fe-doped Co_3O_4 porous NWs clearly, indicating MSI induces a great reduction in the agglomeration of Ru NPs and promotion of the accessibility of active metallic Ru sites. In addition, the corresponding lattice fringe of the samples were measured using HRTEM images as shown in Figs. 1e–h. It was found that a slight increase of the lattice fringe in the FeCo and Ru/FeCo, such as, the FeCo interplanar distance corresponding to (220) was slightly larger than that of Co_3O_4 and the Ru/FeCo (311) interplanar distance was larger than that of Ru/Co_3O_4. The results further proved the doping of Fe cations enter into the Co_3O_4 lattice, which is consistent with the analysis of XRD. Meanwhile, the lattice distortion and expansion of Co_3O_4 can be ascribed to the larger radius of high-spin Fe^{3+} (0.645 Å) compared to high-spin Co^{3+} (0.61 Å) in the newly formed $Co^{2+}{}_{(Td)}$-O-$Fe^{3+}{}_{(Oh)}$ bonds [24]. Fig. 1i shows the HAADF-STEM and EDX elemental maps of Ru/FeCo. All expected elements including Co, Fe and Ru are uniformly distributed within Ru/FeCo, further suggesting that Ru/FeCo catalyst was successfully obtained.

The topography of the catalysts was further investigated by SEM [27,28]. Secondary electron (SE) imaging for Co_3O_4 and Ru/Co_3O_4 shown in Figs. S2a and c (Supporting information) reveal that these two samples presented short rod-like structures, indicating the Ru-loading has very little effect on the morphology. In contrast, smaller and less ordered mesostructured domains were observed in FeCo and Ru/FeCo (Figs. S2b and d in Supporting information), which was in accord with TEM results. The distribution of Co, Fe, O and Ru was also confirmed by the elemental distribution diagram (Fig. S3 in Supporting information), confirming the successful preparation of Ru/FeCo again.

The chemical species and valence states of Co_3O_4, FeCo, Ru/Co_3O_4 and Ru/FeCo were characterized by XPS. The full-spectrum of Ru/FeCo confirms the presence of Ru, Fe, Co and O elements (Fig. S4 in Supporting information), which was consistent with STEM-EDX and SEM-EDX. In the high-resolution XPS spectrum of Co 2p (Fig. 2a), Co $2p_{3/2}$ and Co $2p_{1/2}$ core levels appear at 777.0–785.0 eV and 792.5–801.0 eV, respectively [29,30], and the peaks of Ru/FeCo shift to high binding energy. According to the Gaussian fitting method, the two main peaks can be fitted into four peaks. Among them, the fitting peaks at 797.2 eV and 795.6 eV are attributed to Co^{2+} and Co^{3+} corresponding to the Co $2p_{1/2}$. However, the other two fitting peaks at 781.5 eV and 780.2 eV are associated with the Co^{2+} and Co^{3+} of Co $2p_{3/2}$ [31]. The spin-orbital splitting 15.1 eV and 15.5 eV are characteristic of the existence of both Co^{3+} and Co^{2+}, respectively [32]. In addition, the Co^{2+}/Co^{3+} ratio (Fig. 2e) of Co_3O_4, FeCo, Ru/Co_3O_4 and Ru/FeCo is 0.859, 0.901, 1.255 and 1.313, respectively. It can be concluded that Fe^{3+} mainly occupies the octahedral field of Co^{3+}, in accordance with the decreased proportion of Co^{3+} [23,24], and the MSI of Ru/Co_3O_4 and Ru/FeCo leads to the formation of more defective Co^{2+} sites. In the spectrum of the Fe 2p (Fig. 2b), two distinct peaks are ascribed to Fe $2p_{3/2}$ and Fe $2p_{1/2}$, respectively. The peaks located at around 711.5 eV and 713.8 eV are associated with the Fe^{2+} and Fe^{3+} cations of $2p_{3/2}$ whereas the peaks occurred at around 722.1 eV and 725.8 eV were the characteristic peaks of Fe^{2+} and Fe^{3+} cations of $2p_{1/2}$ [33,34]. Additionally, the satellite peaks ascribed to Fe^{2+} and Fe^{3+} were also observed. Thus the valence of iron in Fe-doped cobalt oxide in this work should be the co-existence of divalent and trivalent. Meanwhile, Ru^0 were detected in both Ru/Co_3O_4 and Ru/FeCo (Fig. 2c), the according peaks of Ru 3p were located at 461.9 eV and 484.2 eV [35]. This positive shift of Ru 3p binding energy is consistent with the positive shift of Co 2p spectrum for Ru/FeCo indicating Fe-doping improves electron transfer between Ru NPs and supports, which helps Ru atoms keep in electron-poor state and is beneficial to the improvement of catalytic activity. The O 1s spectra of all catalysts are presented in Fig. 2d, which is mainly de-convoluted into two peaks corresponding to different oxygen species on the catalysts. As previously reported, the peak at BE of 528.9–530.2 eV and 530.9–531.7 eV were characteristic of lattice oxygen (O_α, *i.e.*, O^{2-}) and defective oxygen (O_β,

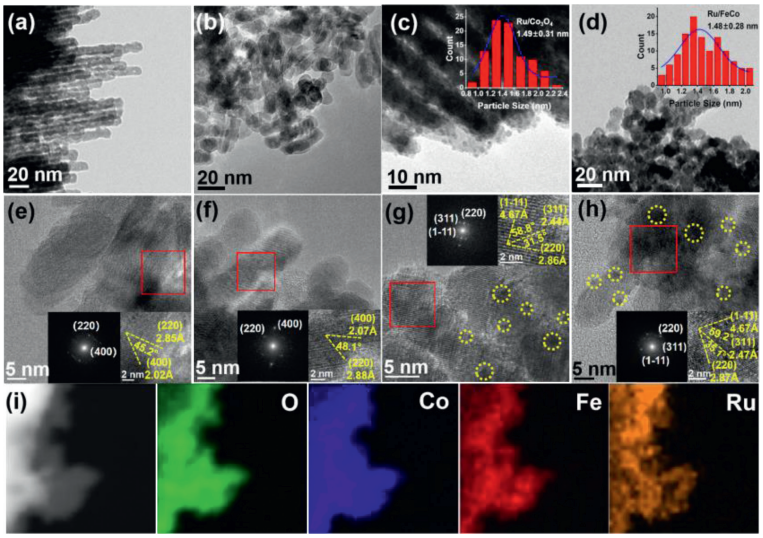

Fig. 1. TEM images of (a) Co_3O_4, (b) FeCo, (c) Ru/Co_3O_4 and (d) Ru/FeCo (insets are the corresponding PSD histograms of Ru NPs). HRTEM images and the corresponding FFTs of (e) Co_3O_4, (f) FeCo, (g) Ru/Co_3O_4 and (h) Ru/FeCo. (i) HAADF-STEM image and the corresponding EDX elemental maps of Ru/FeCo.

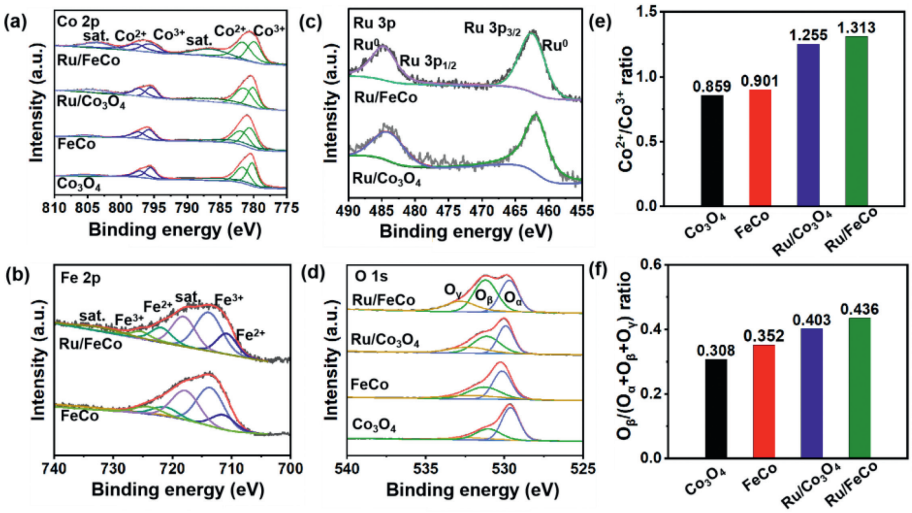

Fig. 2. XPS spectra of (a) Co 2p, (b) Fe 2p, (c) Ru 3p and (d) O 1s. (e) The Co^{2+}/Co^{3+} ratio, (f) the $O_\beta/(O_\alpha+O_\beta+O_\gamma)$ ratio of Co_3O_4, FeCo, Ru/Co_3O_4 and Ru/FeCo.

i.e., O^-, or O_2^{2-}), respectively. Sometimes with a shoulder peak at 532.3–533.1 eV ascribed to hydroxyl species (OH) or adsorbed water species present as contaminants (O_γ) [36–38]. The defective oxygen species $O_\beta/(O_\alpha+O_\beta+O_\gamma)$ ratio (Fig. 2f) was 0.308 in Co_3O_4 catalysts, whereas the Ru/FeCo catalysts presented the ratio with 0.436. The increase in defective oxygen, which indicated that the generation of more oxygen vacancies, can be attributed to the MSI.

The electrocatalytic HER activities of various catalysts including Co_3O_4, FeCo, Ru/Co_3O_4 and Ru/FeCo were evaluated in 1 mol/L KOH in a three-electrode system. It should be noted that all potentials in this work were calculated with iR correction and reported at 10 mA/cm^2 reversible hydrogen electrode (RHE). First, it was explored that the effect of Fe-doping on the electrocatalytic performance of Co_3O_4 NWs for the HER. It can be clearly seen from the linear sweep voltammetry (LSV) curves (Fig. 3a) and the required overpotential to achieve a current density of 10 mA/cm^2 (Fig. 3b and Table S1 in Supporting information) that the introduction of Fe showed a remarkable decrease from 484 mV to 361 mV in the overpotential values of Co_3O_4. After the loading of Ru NPs, the catalytic performances of Ru/Co_3O_4 and Ru/FeCo enhanced significantly owing to their proven efficiency for the HER. In particular, the overpotential of Ru/FeCo was at 155 mV for 10 mA/cm^2, which was much lower than that of Ru/Co_3O_4 (226 mV) and FeCo (361 mV), demonstrating the effectiveness of combining iron doping and Ru anchoring onto Co_3O_4 NWs. Similarly, Fig. 3c compares the current densities obtained at a constant potential of 250 mV. As can be seen from these figures, the pure Co_3O_4 without any modification exhibited very poor electrocatalytic activity toward HER while the Ru/FeCo catalyst showed outstanding performance.

The HER kinetics were probed from the linear fitting of the Tafel plots (Fig. 3d) [39]. As known, a smaller Tafel slope indicates the fast catalytic kinetics due to a great increase of the electrocatalytic current density [40–42]. The Tafel slope of the FeCo was measured to be 88.35 mV/dec, which was lower than that of the Co_3O_4 (95.47 mV/dec), indicating better catalytic kinetics of Fe-doped Co_3O_4. As expected, Ru/FeCo had the lowest Tafel slope value (82.81 mV/dec), indicating the relatively rapid HER kinetics among the as-prepared samples. Meanwhile, the electrochemical impedance spectroscopy (EIS) tests were used to evaluate charge transfer kinetics of different catalysts [43,44]. Small R_{ct} indicates excellent charge transfer ability of catalysts [45]. As shown in the

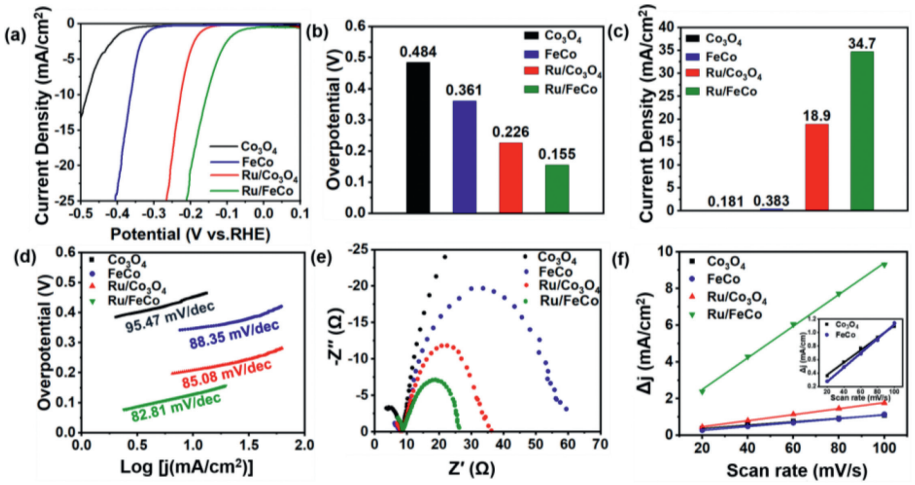

Fig. 3. (a) LSV curves, (b) overpotential values (@10 mA/cm^2), (c) current densities (@250 mV), (d) Tafel plots, (e) EIS Nyquist plots and (f) current density difference (Δj) plot as a function of scan rates to calculate the double-layer capacitance value (C_{dl}) of Co_3O_4, FeCo, Ru/Co_3O_4 and Ru/FeCo for HER (the inset is the magnification of Co_3O_4 and FeCo plot).

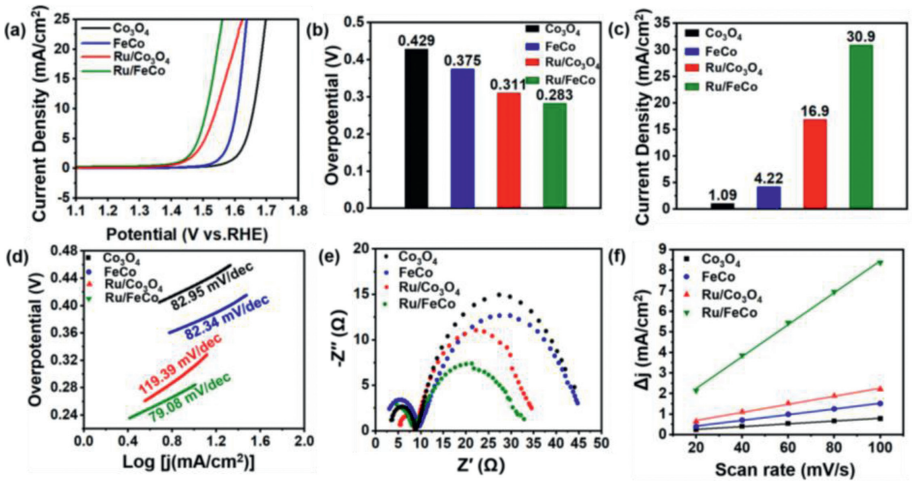

Fig. 4. (a) LSV curves, (b) overpotential values (@10 mA/cm^2), (c) current densities (@350 mV), (d) Tafel plots, (e) EIS Nyquist plots and (f) current density difference (Δj) plot as a function of scan rates to calculate the double-layer capacitance value (C_{dl}) of Co_3O_4, FeCo, Ru/Co_3O_4 and Ru/FeCo for the OER.

Nyquist plots (Fig. 3e), FeCo has a lower charge transfer resistance compared to pure Co_3O_4. This is due to incorporating iron is beneficial to enhance electron transfer on the electrical double layer [46]. Promisingly, the Ru/FeCo showed the lowest R_{ct} (~17 Ω) in Table S1. This result is in excellent agreement with the findings from the LSV and Tafel plots, suggesting excellent electrocatalytic activity for the HER.

To further evaluate the intrinsic HER activity of the Ru/FeCo catalyst, it was measured that the electrochemical double-layer capacitance (C_{dl}) from the cyclic voltammetry (CV) as a function of scan rate (20–100 mV/s) (Fig. S5 in Supporting information) [47,48]. It is well established that C_{dl} is linearly proportional to the electrochemically surface area (ECSA) of the catalysts [47,49,50]. The C_{dl} value of Ru/FeCo was determined to be 86.24 mF/cm^2 (Fig. 3f), which was significantly higher than those of Co_3O_4, FeCo and Ru/Co_3O_4, revealing the outstanding electrochemically active area with highly exposed catalytic active sites of the Ru/FeCo for the HER.

OER activities were also examined by observing the overpotential at 10 mA/cm^2 in 1 mol/L KOH electrolyte under the same condition. The LSV curves of four catalysts above are displayed in Fig. 4a. The trend in the overpotential for OER is the same as that for HER, which can be concluded as Ru/FeCo (283 mV) < Ru/Co_3O_4 (311 mV) < FeCo (375 mV) < Co_3O_4 (429 mV) (Fig. 4b and Table S2 in Supporting information), suggesting that the Ru/FeCo catalyst has the most excellent OER activity among four catalysts. The current densities obtained at a constant potential of 350 mV (Fig. 4c) were compared, it can be seen that Ru/FeCo has the highest current density with the value of 30.9 mA/cm^2. In Fig. 4d and Table S2, the Tafel slope of Ru/FeCo was 79.08 mV/dec, which is smaller than that of other three catalysts, suggesting a favorable OER kinetics on Ru/FeCo. Regarding to the charge transfer kinetics of catalysts for OER, Ru/FeCo displays the smallest R_{ct} (~25 Ω) in Fig. 4e and Table S2, indicating the MSI between Ru and FeCo enhanced the charge transfer ability of Ru/FeCo. The intrinsic OER activity of Ru/FeCo catalyst was also evaluated by the C_{dl} from the CV (Fig. S6 in Supporting information). As shown in Fig. 4f and Table S2, the C_{dl} of Ru/FeCo (77.62 mF/cm^2) goes up dramatically, suggesting that MSI makes the Ru/FeCo have a lager electrochemically active area, which can expose more catalytic active sites for OER.

The stability of catalysts is a key factor for their practical application. It was examined by current-time curve method at 0.8 V (*vs.* RHE) for Ru/FeCo catalyst in alkaline solution (1 mol/L KOH) (Figs. S7a in Supporting information). The i-t curve shows negligible attenuation after a long period of 20 h test, demonstrating that the Ru/FeCo catalyst has excellent long-term electrochemical durabil-

ity. The oscillation phenomenon of the current density shown in the partial enlarged detail (insert of Fig. S7a) was due to the large number of bubbles generated on the electrode surface during the *i-t* test. Furthermore, TEM and HRTEM images of the used catalysts were performed in the locations with less-visible amorphous phase of Nafion binder. As shown in Figs. S7b-e (Supporting information), the mesostructured NW morphology of Ru/FeCo are maintained, and no structural collapse occurs. Compared to the fresh catalysts, the bulk region of used samples maintains the high crystallinity with similar lattice spacing. It indicates that Ru/FeCo catalyst has good structural stability and reusability, mainly thanks to the strong interactions developed between Ru NPs and FeCo support.

In summary, the optimized Ru/FeCo catalyst is developed as a bifunctional electrocatalyst for efficient water splitting. A series of physical characterization and chemical tests show that the ultrasmall Ru NPs (~1.48 nm) are uniformly distributed on the supports, and the overpotential of HER at 10 mA/cm^2 is 155 mV, while the overpotential of OER at 10 mA/cm^2 is 283 mV. In addition, the Ru/FeCo catalyst has excellent long-term electrochemical durability in 1 mol/L KOH solution, and no significant changes were found in the structural comparison of the catalysts before and after the reaction. These excellent properties can be attributed to the abundant metal-support interactions in Ru/FeCo, which enhance the charge transfer between Ru and FeCo support resulting in modified electronic structure of Ru NPs to facilitate the electrochemical reactions. This work provides a guideline for the design of high-efficiency bifunctional electrocatalysts.

Declaration of competing interest

The authors declare that they have no known competing financial interests or personal relationships that could have appeared to influence the work reported in this paper.

Acknowledgments

The authors gratefully acknowledge the financial support provided by the National Natural Science Foundation of China (Nos. 52161145403, 22072164, 51932005), Liaoning Revitalization Talents Program (No. XLYC1807175), and the Research Fund of Shenyang National Laboratory for Materials Science.

Supplementary materials

Supplementary material associated with this article can be found, in the online version, at doi:10.1016/j.cclet.2022.108085.

References

[1] S. Chu, A. Majumdar, Nature 488 (2012) 294–303.
[2] M.W. Kanan, D.G. Nocera, Science 321 (2008) 1072–1075.
[3] H. Sun, C.W. Tung, Y. Qiu, et al., J. Am. Chem. Soc. 144 (2022) 1174–1186.
[4] J. Yang, W. Li, D. Wang, Y. Li, Adv. Mater. 32 (2020) 2003300.
[5] C.J. Pan, M.C. Tsai, W.N. Su, et al., J. Taiwan Inst. Chem. Eng. 74 (2017) 154–186.
[6] G. Wehmeyer, T. Yabuki, C. Monachon, J. Wu, C. Dames, Appl. Phys. Rev. 4 (2017) 041304.
[7] J. Mahmood, F. Li, S.M. Jung, et al., Nat. Nanotechnol. 12 (2017) 441–446.
[8] Q. Wang, M. Ming, S. Niu, et al., Adv. Energy Mater. 8 (2018) 1801698.
[9] M. Bat-Erdene, M. Batmunkh, B. Sainbileg, et al., Small 17 (2021) 2102218.
[10] X. Sun, X. Gao, J. Chen, et al., ACS Appl. Mater. Interfaces 12 (2020) 48591–48597.
[11] Z. Liu, L. Zeng, J. Yu, et al., Nano Energy 85 (2021) 105940.
[12] T.Y. Ma, S. Dai, M. Jaroniec, S.Z. Qiao, J. Am. Chem. Soc. 136 (2014) 13925–13931.
[13] J. Bao, X. Zhang, B. Fan, et al., Angew. Chem. Int. Ed. 54 (2015) 7399–7404.
[14] Z.W. Gao, J.Y. Liu, X.M. Chen, et al., Adv. Mater. 31 (2019) 1804769.
[15] Y. Liu, X. Zhang, W. Zhang, et al., Energy Environ. Mater. (2022), https://doi.org/10.1002/eem2.12438.
[16] J. Wellendorff, T.L. Silbaugh, D. Garcia-Pintos, et al., Surf. Sci. 640 (2015) 36–44.
[17] Y. Yao, S. Hu, W. Chen, et al., Nat. Catal. 2 (2019) 304–313.
[18] T. Tang, W.J. Jiang, S. Niu, et al., J. Am. Chem. Soc. 139 (2017) 8320–8328.
[19] X. Long, J. Li, S. Xiao, et al., Angew. Chem. Int. Ed. 53 (2014) 7584–7588.
[20] D. Yan, R. Chen, Z. Xiao, S. Wang, Electrochim. Acta 303 (2019) 316–322.
[21] K.L. Yan, J.F. Qin, J.H. Lin, et al., J. Mater. Chem. A 6 (2018) 5678–5686.
[22] X. Zhu, D. Hou, H. Tao, M. Li, J. Alloy. Compd. 821 (2020) 153580.
[23] E. Budiyanto, M. Yu, M. Chen, et al., ACS Appl. Energy Mater. 3 (2020) 8583–8594.
[24] X. Gao, J. Liu, Y. Sun, et al., Inorg. Chem. Front. 6 (2019) 3295–3301.
[25] L.C.E. da Silva, A. Cassago, L.C. Battirola, M.D.C. Gonçalves, R.V. Portugal, Cellulose 27 (2020) 5435–5444.
[26] A. Gujrati, S.R. Khanal, L. Pastewka, T.D.B. Jacobs, ACS Appl. Mater. Interfaces 10 (2018) 29169–29178.
[27] Y. Wang, S. Sun, Fuel 289 (2021) 119915.
[28] L. Wang, W. Zhou, Z. Yu, et al., ACS Appl. Mater. Interfaces 13 (2021) 15017–15030.
[29] A. Wang, Y. Shi, L. Yang, G. Fan, F. Li, Catal. Commun. 153 (2021) 106302.
[30] A. Ashok, A. Kumar, J. Ponraj, S.A. Mansour, F. Tarlochan, Appl. Catal. B: Environ. 254 (2019) 300–311.
[31] J. Xu, X. Zhong, X. Wu, Y. Wang, S. Feng, J. Energy Chem. 71 (2022) 129–140.
[32] J.J. Beltrán, C.A. Barrero, A. Punnoose, J. Phys. Chem. C 118 (2014) 13203–13217.
[33] X. Zou, W. Zhang, X. Zhou, K. Song, et al., J. Energy Chem. 72 (2022) 509–515.
[34] A. Abdelmoneim, A. Naji, E. Wagenaars, M. Shaban, Int. J. Hydrog. Energy 46 (2021) 12915–12935.
[35] X. Gao, B. Li, X. Sun, et al., Chin. Chem. Lett. 32 (2021) 3591–3595.
[36] C. Wang, C. Zhang, W. Hua, et al., RSC Adv. 6 (2016) 99577–99585.
[37] Y. Lao, N. Zhu, X. Jiang, et al., Catal. Sci. Technol. 8 (2018) 4797–4811.
[38] X.W. Lv, Y. Liu, W. Tian, L. Gao, Z.Y. Yuan, J. Energy Chem. 50 (2020) 324–331.
[39] T.M. Freire, R.M. Freire, M.L. Franco, et al., Mater. Today Sustain. 18 (2022) 100150.
[40] M. Zeng, Y. Li, J. Mater. Chem. A 3 (2015) 14942–14962.
[41] Y. Li, X. Hu, J. Huang, et al., Acta Phys. Chim. Sin. 37 (2021) 25–26.
[42] M. Yao, H. Hu, B. Sun, et al., Small 15 (2019) 1905201.
[43] S. Anantharaj, S. Noda, ChemElectroChem 7 (2020) 2297–2308.
[44] M.A. Hefnawy, S.A. Fadlallah, R.M. El-Sherif, S.S. Medany, J. Alloy. Compd. 896 (2022) 162857.
[45] Y. Xia, Y. Pei, Y. Hu, et al., Acta Phys. Chim. Sin. 37 (2021) 180–186.
[46] E. Budiyanto, M. Yu, M. Chen, et al., ACS Appl. Energy Mater. 3 (2020) 8583–8594.
[47] L. Wu, J.P. Hofmann, ACS Energy Lett. 6 (2021) 2619–2625.
[48] Z. Ren, Y. Han, N. Cong, et al., J. Electroanal. Chem. 848 (2019) 113320.
[49] L. Lu, Q. Li, J. Du, W. Shi, P. Cheng, Chin. Chem. Lett. 33 (2022) 2928–2932.
[50] S. Xiong, P. Li, Z. Jin, et al., Electrochim. Acta 222 (2016) 999–1006.